archives
of thermodynamics
Vol. **41**(2020), No. 3, 57–89
DOI: 10.24425/ather.2020.134572

Augmentation in heat transfer and friction of three sides over one side dimple roughened solar duct

VIKASH KUMAR*

Department of Mechanical Engineering, Maulana Azad National Institute of Technology (MANIT)-Bhopal, MP-462003, India

Abstract Providing roughness is an effective method to heat fluids to high temperature. Present paper make use of concave dimple roughness on one and three sides of roughened ducts aimed at determining rise in heat transfer and friction of three sides over one side roughened duct. Three sides roughened duct produces high heat transfer compared to one side roughened. Results are shown as a rise in Nusselt number and friction factor of three sides over one side roughened duct. Experimental investigation was conducted under actual outdoor condition at National Institute of Technology Jamshedpur, India to test various sets of roughened collectors. Roughness parameter varied as relative roughness pitch 8–15, relative roughness height 0.018–0.045, dimple depth to diameter ratio 1–2, Reynolds number 2500–13500 at fixed aspect ratio (width/hight) 8. Highest enhancement in Nusselt number for varying relative roughness pitch, height, and diameter ratio was respectively found as 2.6 to 3.55 times, 1.91 to 3.42 times and 3.09 to 3.94 times compared to one side dimple roughened duct. Highest rise in friction for three sides over one side roughened duct for these varying parameters was respectively found as 1.62 to 2.79 times, 1.52 to 2.34 times and 2.21 to 2.56 times. To visualize the effect of roughness parameter on heat transfer and friction factor, variation in Nusselt number and friction factor for varying roughness parameters with Reynolds number is shown.

Keywords: Dimple roughened; Relative roughness pitch; Relative roughness height; Dimple depth to diameter ratio; Nusselt number; Friction factor

*Corresponding Author. Email: vikashism2012@gmail.com

Nomenclature

A_o	–	area of orifice of orifice plate,m^2
A_p	–	area of absorber plate, m^2
C_d	–	coefficient of discharge
C_p	–	specific heat capacity of air, J/kgK
D_h	–	hydraulic diameter of duct, m
d	–	dimple diameter, m
e	–	dimple depth/height, m
H	–	height of SAH duct, m
h	–	convective heat transfer coefficient
k	–	thermal conductivity of air, W/m K
L	–	length of SAH duct, m
$\dot{m}$	–	mass flow rate of air, kg/s
p	–	dimple pitch, m
Δp_d	–	test section pressure drop, N/m^2
Δp_o	–	orifice meter pressure drop, N/m^2
Q_u	–	useful heat gain, W
SAH	–	solar air heater
T_{pm}	–	mean absorber plate temperature, °C
T_{fm}	–	mean air temperature in the duct, °C
v_d	–	average velocity of air through the duct, m/s
W	–	width of SAH duct, m

Greek symbols

β	–	ratio of outer diameter of orifice plate to its inner diameter
μ	–	dynamic viscosity of air, Ns/m^2
ν	–	kinematic viscosity of air, m^2/s
ρ	–	density, kg/m^3

Dimensionless parameters

p/e	–	relative roughness pitch
e/D_h	–	relative roughness height
e/d	–	dimple depth to diameter ratio
f	–	friction factor
f_{1r}	–	friction factor for one side roughened duct
f_{3r}	–	friction factor for three sides roughened duct
Nu	–	Nusselt number
Nu_{1r}	–	Nusselt number for one side roughened duct
Nu_{3r}	–	Nusselt number for three sides roughened duct
Re	–	Reynolds number
W/H	–	aspect ratio of collector duct

Subscripts

$1r$	–	one side roughened
$3r$	–	three sides roughened
a	–	air
f	–	fluid
i	–	inlet
o	–	outlet

1 Introduction

Artificially roughened solar air heater (SAH) is being widely used worldwide to heat air from ambient temperature to high temperature around 70–80 °C. It makes use of absorber plates with roughness that grasps thermal energy of solar insolation and further transfers that energy to flowing air underside [1]. The value of convective heat transfer coefficient (h) and heat capacity (C_p) for air is low that results in reduced heat transfer from the plate to air. Many researchers have used solar air heaters of different configurations to remove these drawbacks [2, 3]. Roughened solar duct works on principle that whenever air flows under action of blower/fan beneath heated surface, flow is turbulent. In turbulent zone, there exists viscous sublayer near surface. Thickness of viscous sublayer is very much less than thickness/height of roughness element provided. In that viscous sublayer, flow remains laminar. In laminar zone, there is less transfer of heat from heat transferring surface to under flowing air. Roughness is provided to artificially destroy viscous sublayer to obtain highest heat transfer from the absorber surface [4–6].

However, excessive turbulence eventually leads to more power requirement from the fan/blower to suck air through roughened duct [7]. To minimize friction losses, special care should be taken while selecting dimensions for roughness geometries. Literature reveals that roughness should be provided very close to heat transfer surface (height/depth of roughness element should not exceed laminar sublayer thickness) because if roughness's dimension exceeds laminar sublayer thickness, there may be drastic increase in pumping power requirement, reducing overall performance of roughened SAH duct [8–12].

Prasad and Saini used artificially roughened small diameter wires of $e/D_h = 0.020-0.033$ and $p/e = 10-20$ for the Reynolds number (Re) between 5000 and 50 000 [13]. Results showed that mean value of Nu and f increased with increase in e/D_h value. Ravigururajan and Bergles derived correlations for the Nusselt number (Nu) and friction factor (f) for flow under rib-roughened tubes [14]. Lau *et al.* [9] performed comparison studies on full/staggered discrete ribs arrays and concluded that for fixed value of pumping power, 60° and 45° discrete ribs were respectively responsible for augmenting the heat transfer by 5–19% and 11–32% compared to full ribs. Saini and Saini used expanded mesh roughened absorber that yielded Nu, f, and thermal efficiency (ν_{th}) enhancement of 4 times, 5 times and 37–57%, respectively [15]. Momin *et al.* [16] used V-shape as roughness

with relative roughness height (e/D_h) 0.02–0.034, the angle of flow attack (α) 30°–90° and Re 2500–18 000. Highest enhancement in Nu and f was observed as 2.30 and 2.83 times of that of non-roughened duct for the angle of flow attack of 60°. Karmare and Tikekar studied Nu and f characteristics in metal grit roughened SAH and found that highest augmentationin Nu and f was 187% and 213%, respectively [17]. Chandra *et al.* [18] investigated square duct roughened with transverse ribs on 1, 2, 3, and 4 walls of the duct. The flow Re varied from 10 000 to 80 000, $e/D_h = 0.0625$ and $p/e = 8$, heat transfer was enhanced by 2.16 for one ribbed wall and 2.57 for four ribbed wall. Burgess *et al.* [19] studied effects of dimple depth on Nu and f and found that increasing depth of dimple to print diameter (e/d) from 0.1 to 0.3, convective heat transfer coefficient value (h) increased due to introduction of intensified vortices and secondary flows ejecting from dimples. Ridouane and Campo [20] investigated computationally Nu and f characteristics of air flowing under parallel-plate transverse semi-cylindrical cavities and found enhancement in heat transfer by 30% relative to smooth duct and pressure loss increments by 19%. Karwa *et al.* [21] experimentally studied integral chamfered rib (transverse pattern) roughened absorber plate and observed twofold increase in Stanton number and 3-fold increase in f as compared to the smooth duct. Jaurker *et al.* [22] used rib-grooved roughened SAH and found enhancement in Nu and f as 2.7 and 3.6 times respectively compared to non-roughened ducts. Saini and Saini used arc shape roughness element and reported rise in Nu and f as 3.6 and 1.75 times, respectively, compared to non-roughened duct for $\alpha/90$ of 0.3333 and e/D_h of 0.0422 [23]. Wongcharee *et al.* [24] analyzed differently oriented ribs and observed that cylindrical ribs provided highest enhancement in thermohydraulic performance and lowest enhancement in Nu for rectangular ribs. Varun *et al.* [25] investigated Nu and f using roughness element as combination of inclined and transverse ribs. For $p/e = 8$, thermal performance obtained was highest. Provision of roughness was not only limited to one wall but it extended beyond that. Study reported by Kumar and Prasad [26–28] using three roughened walls reveals that augmentation in thermal efficiency of three sides over one side roughened duct is 44–56% for varying p/e and 39–51% for varying e/D_h. In another study reported by Kumar and Prasad, correlations for Nu and f were derived and performance analysis was done for three sides roughened duct [29–33].

It appears from literature that highest roughness provided were limited to one side while remaining sides were insulated. This paper is aimed at

determining augmentation in Nu and f for three sides over one side dimple roughened solar duct. If roughness provided is on all three sides, (2 side walls and 1 top wall), they can participate in the heat transfer augmentation process accompanied by the slightest increase in pressure drop.

2 Experimentation and roughness geometry parameters

Figure 1 depicts schematic diagram of test set-up used under present investigation. Figure 2 depicts actual photograph of test rig designed and fabricated at terrace of Mechanical Engineering Department, NIT Jamshedpur. Figure 3 shows photograph of dimple roughened absorber plate. Figure 4 shows sectional view of dimple roughness geometry. Ten sets of roughened plates were fabricated as per ASHRAE standard [34]. The experimental set-up has three ducts, A, B and C with provision to accommodate one-side roughened, non-roughened (smooth) and three-sides roughened absorber simultaneously.

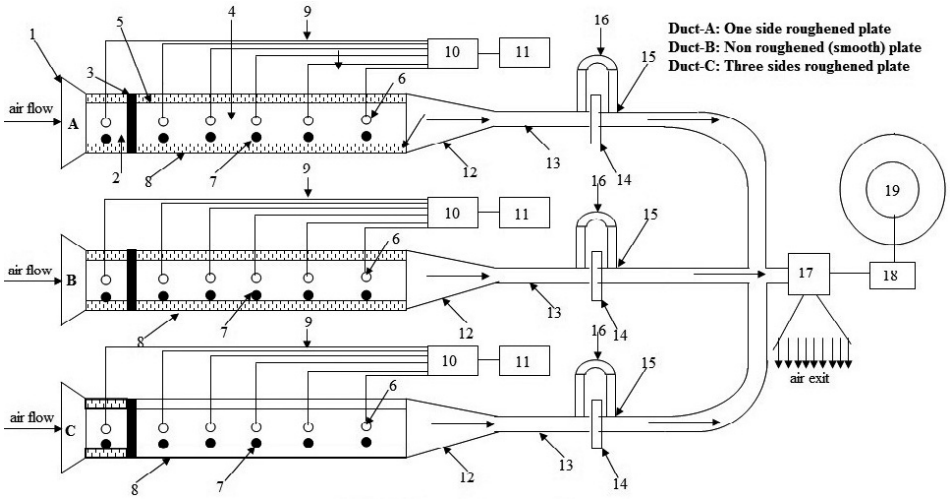

Figure 1: Schematics of test set-up. 1 – trapezoidal air inlet, 2 – non-roughened duct section, 3 – insulation between entry and test length, 4 – roughened duct section, 5 – insulation, 6 – thermocouple, 7 – thermometer, 8 – glass covers, 9 – copper wire, 10 – selector switch, 11 – digital voltmeter, 12 – converging section, 13 – cylindrical pipe, 14 – orifice-plate, 15 – flange couplings, 16 – U-tube manometer, 17 – blower, 18 – motor, 19 – auto-variac.

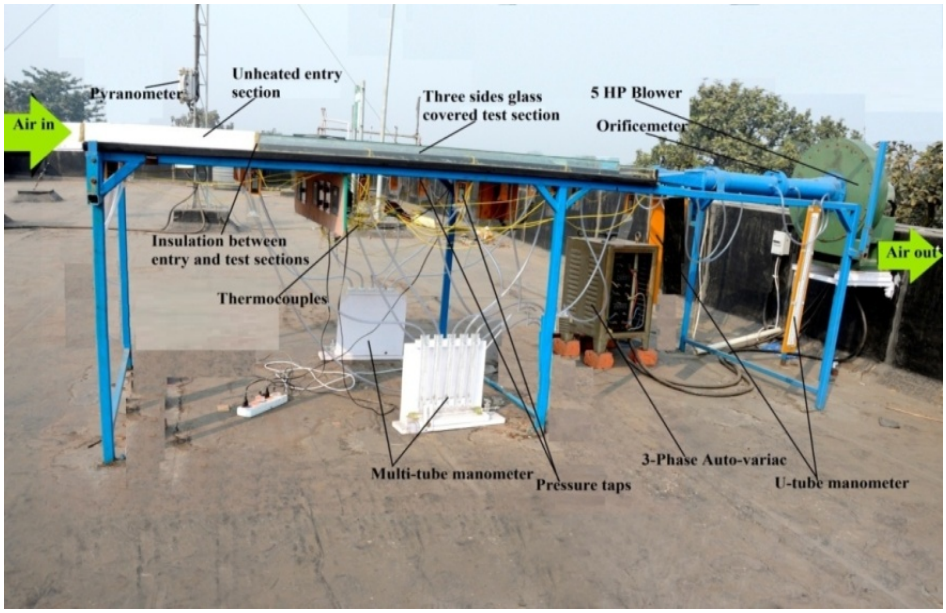

Figure 2: Photograph of test setup.

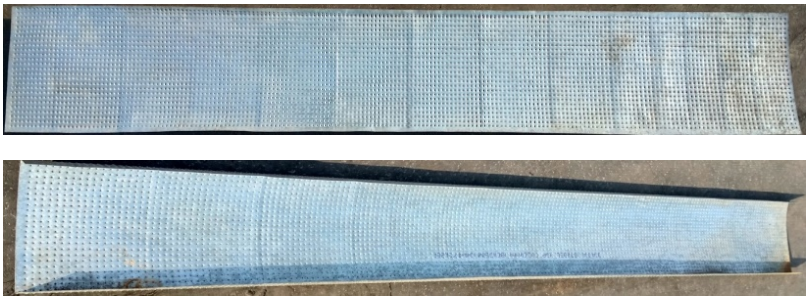

Figure 3: Photograph of one and three sides roughened absorber plates.

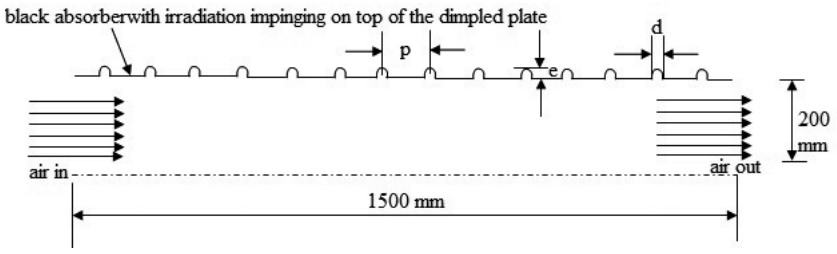

Figure 4: Sectional view of a concave dimple roughened absorber plate.

The two ducts are made similar in all dimensions to compare Nu and f characteristics. A (2130 × 630) mm wooden piece 25 mm thick act as common bottom plate for ducts, side walls 50 mm × 50 mm wooden piece. 3-sides roughened duct has one side insulation and three sides glass covers. Figure 5 shows the schematic view of the two ducts used under present investigation. The flow under a typical 3-sides dimple roughened collector is depicted in Fig. 6.

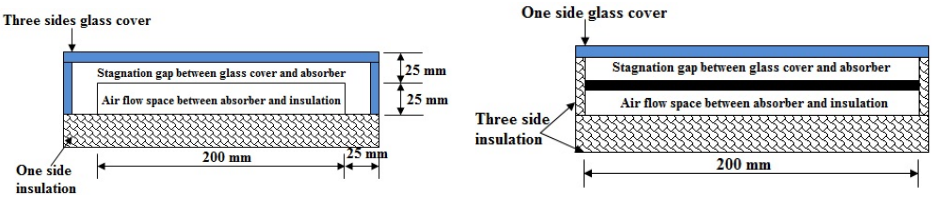

(a) (b)

Figure 5: Schematics of the artificially roughened ducts (a) three sides roughened duct with one sides insulation, (b) one side roughened duct with three sides insulation.

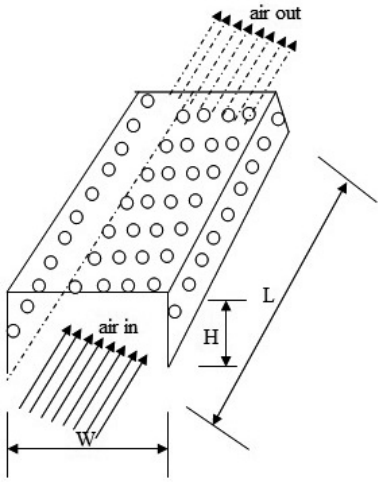

Figure 6: Flow under typical three sides dimple roughened absorber plate.

Calibrated copper-constantan thermocouples (28 SWG (British) Standard Wire Gage) with digital microvoltmeter output in degrees Celsius (°C) having least count 0.1 °C is used to measure collector's temperatures. Eighteen thermocouples is soldered on top surface of collector to record col-

lector's temperatures. Six among eighteen thermocouples were soldered on top surface of one side roughened duct and remaining twelve were equally distributed on top and side wall of three sides roughened duct, six being on top wall and six on the side wall. The positioning of thermocouples is depicted in Figs. 7 and 8. Digital thermometers were inserted through bottom side of duct at six different locations to record heated air temperature flowing as shown in Fig. 9. The flow and roughness geometry parameters used under present study is presented in Tab. 1. Solar radiations intensity, wind speed, ambient air temperature, and atmospheric pressure were directly recorded from digital display of pyranometer system.

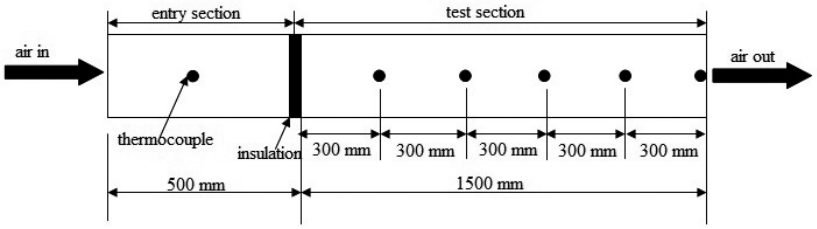

Figure 7: Thermocouple positioning on one side roughened absorber plate.

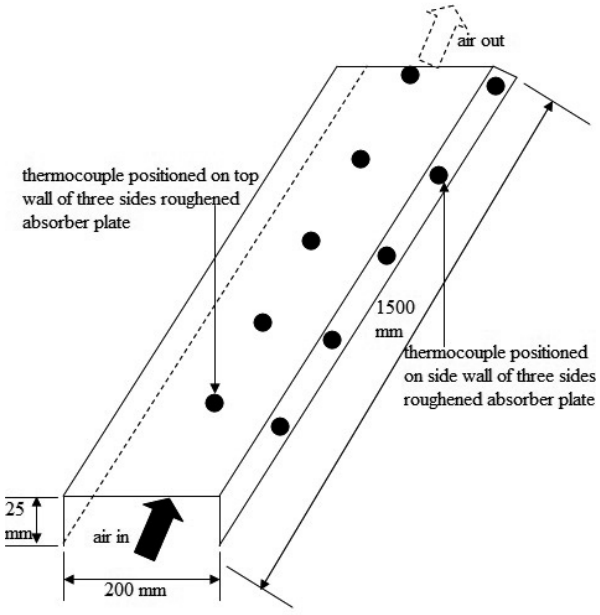

Figure 8: Thermocouple positioning on three sides roughened absorber plate.

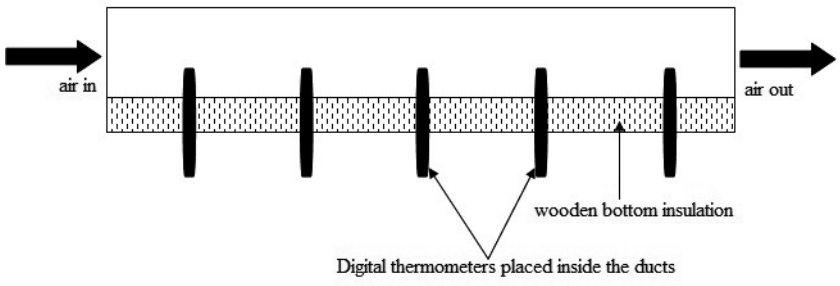

Figure 9: Digital thermometers placed inside air flow duct test section.

The flow and roughness geometry parameters used under present study is presented in Tab. 1.

Table 1: Range of flow and geometrical parameters.

Flow and Geometrical Parameters (Variable Value Range)			
Relative roughness pitch	p/e	–	8–15
Relative roughness height	e/D_h	–	0.018–0.045
Depth to diameter ratio	e/d	–	1–2
Reynolds number	Re	–	2500–13500
Intensity of solar radiation	I	W/m^2	720–980
Atmospheric temperature	T_a	°C	24–44
Wind velocity	W_v	m/s	0.2–3.5

3 Experimentatal procedure

Heated air and collector's temperatures were recorded at different locations in duct were used for determining the values of different parameters.

3.1 Mean plate and air temperatures

The mean temperatures, T_{pm} and T_{fm}, are simply the arithmetic mean of temperatures at different locations in between the inlet and exit. Thus

$$(T_{pm})_{3r} = \frac{T_1 + T_2 + \ldots + T_{12}}{12}, \tag{1}$$

$$(T_{pm})_{1r} = \frac{T_1 + T_2 + \ldots + T_6}{6}, \tag{2}$$

$$(T_{fm})_{3r} = \frac{T_1 + T_6}{2}\,, \tag{3}$$

$$(T_{fm})_{1r} = \frac{T_1 + T_6}{2}\,. \tag{4}$$

3.2 Mass flow rate measurement

The flow rate of air under roughened plate is calculated as

$$\dot{m} = C_d A_o \left[\frac{2\rho\Delta p_o}{1-\beta^4}\right]^{0.5}. \tag{5}$$

3.3 Friction factor

The friction factor value across test section length 1500 mm with pressure taps inserted at five different locations, each at a gap of 300 mm is calculated as

$$f = \frac{(\Delta p)_d\, D_h}{2\rho L v_d^2}\,, \tag{6}$$

where v_d is the flow velocity of air and D_h is the hydraulic diameter for the duct

$$D_h = \frac{4WH}{[2(W+H)]}\,. \tag{7}$$

3.4 Reynolds Number

The Re is calculated using

$$\mathrm{Re} = \frac{v_d D_h}{\upsilon}\,. \tag{8}$$

3.5 Heat transfer coefficient

Useful heat gain of air is given by

$$Q_u = \dot{m} C_p\,(T_6 - T_1)\,. \tag{9}$$

The convective heat transfer coefficient for the heated test section has been calculated from

$$h = \frac{Q_u}{A_p\,(T_{pm} - T_{fm})}\,. \tag{10}$$

3.6 Nusselt Number

The convective heat transfer coefficient is used to determine the Nusselt number and is determined as

$$\mathrm{Nu} = \frac{hD_h}{k}\,. \tag{11}$$

4 Validation of experimental data

Experiments were carried and data were recorded for non-roughened, one side roughened and three sides roughened duct. One side concave dimple roughened duct used in present study is similar to those of Saini and Verma [35]. Correlation for the Nusselt number and friction factor derived by them are worth to be valid for present geometry to compare values of Nusselt number obtained in present study with values obtained from correlations [37]. Figure 10 shows the validity curve for test rig.

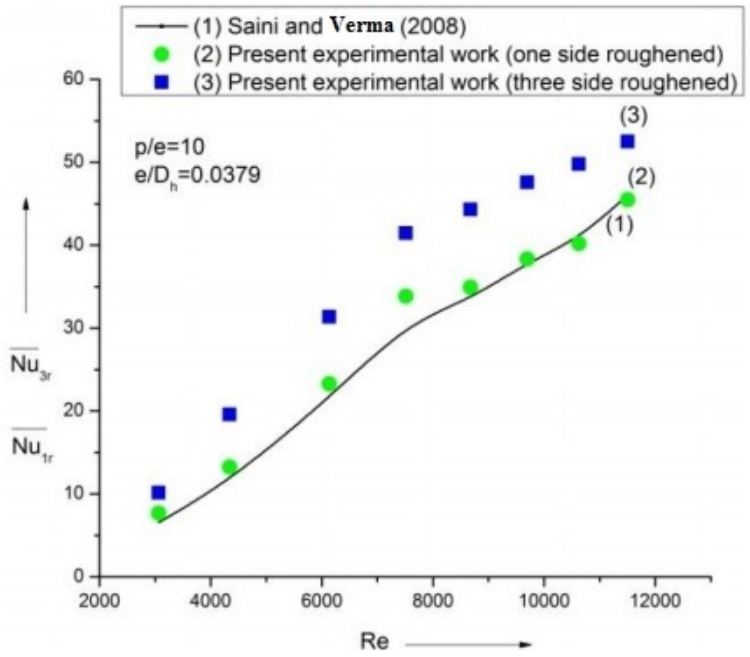

Figure 10: Validation of the test rig.

$$(\mathrm{Nu})_{1r} = 5.2 \times 10^{-4} \times (\mathrm{Re})^{1.27} \times \left(\frac{p}{e}\right)^{1.15} \times \left(\frac{e}{D_h}\right)^{0.0333} \left[\exp(-2.12)\left(\log\left(\frac{p}{e}\right)\right)^2\right] \left[\exp(-1.30)\left(\log\left(\frac{e}{D_h}\right)\right)^2\right]. \quad (12)$$

One side dimple roughened data compared well with similar model taken by Saini and Verma, therefore, results for three sides roughened ones are worth to be valid and hence been utilized further. The values of Nusselt number determined from experimentation were in reasonable agreement with values computed from correlations. The mean deviation in calculated and experimental of Nusselt number and friction factor was ±3.7% for Nu and ±4.5% for f.

4.1 Uncertainty analysis

There are always chances of errors in measurement of experimental data regardless of care taken. It is, therefore, essential to analyze the system to determine the highest possible error and hence the validity of experimental measurements. A procedure for estimating uncertainty in measurement of data has been described in Appendix-A. Based on method of Kline and McClintock for calculating uncertainties [36], the uncertainties associated with various parameters have been calculated and tabulated in Tab. 2. Errors in measurement of various measuring instrument are tabulated in Tab. 3.

Table 2: Uncertainties in measurement of various parameters.

Name of parameter	Symbol	Uncertainty range (%)
Area of absorber plate	A_p	0.07
Cross sectional area of air flow duct	A	0.16
Area of orifice meter	A_o	0.21
Hydraulic diameter	D_h	0.23
Density	ρ	0.106
Mass flow rate	$\dot{m}$	0.84
Velocity of air through test section	v_d	0.86
Reynolds number	Re	0.9
Heat transfer coefficient	h	3.724
Nusselt number	Nu	4.167
Friction factor	f	4.389

Table 3: Error associated with different measuring instruments.

Measurement Parameter	Symbol	Instrument	Least Count	Error
Length	L	Linear scale	1 mm	±1 mm
Duct height	H	Vernier scale	0.05 mm	±0.13 mm
Duct width	W	Linear scale	0.05 mm	±0.07 mm
Diameter of orifice meter	D_2	Vernier scale	0.05 mm	±0.09 mm
Temperature measurement	T	Digital thermometer	–	±0.35 °C
Pressure drop across test section	Δp_d	Multitube manometer	1 mm of H_2O	±1 mm
Pressure drop across orifice meter	Δp_o	U-tube manometer	1 mm of H_2O	±2 mm
Global radiation	I	Pyranometer	–	±19 W/m^2

5 Results and discussions

Figure 11 and 12 respectively shows variation in ambient condition and change in air and plate temperature. Solar radiation intensity increases up to 1.00 pm after which it decreases. The highest and lowest value of global radiation obtained during experimental day is 923 and 714 W/m^2. Roughness provided on collector's surface leads higher heat exchange between plate and air. Plate temperature decreases and air temperature increases.

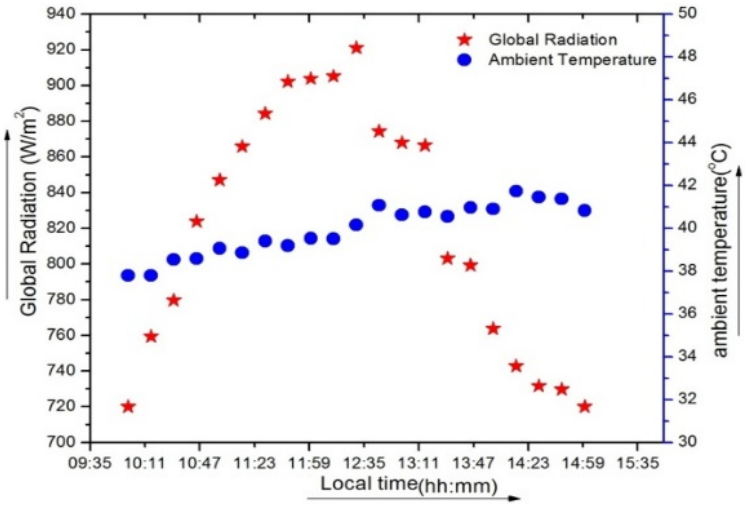

Figure 11: Typical variation in ambient condition on a clear sky day.

Rise in air temperature for three sides roughened duct is more than temperature rise for one side roughened duct because heat transfer in three sides roughened duct is more than one side roughened duct.

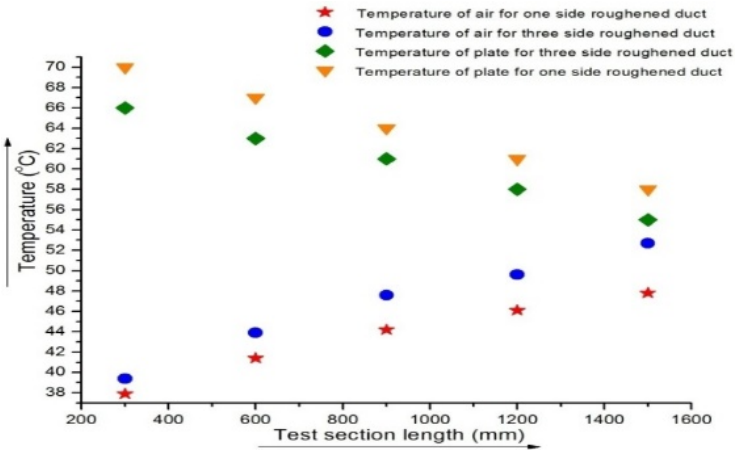

Figure 12: Variation in temperature of plate and air along test length.

5.1 Effect of relative roughness pitch on Nusselt number

Figure 13 shows the effect of p/e on Nusselt number for constant $e/D_h = 0.036$ and $e/d = 1.5$. It is evident from the figure that as Re is increased,

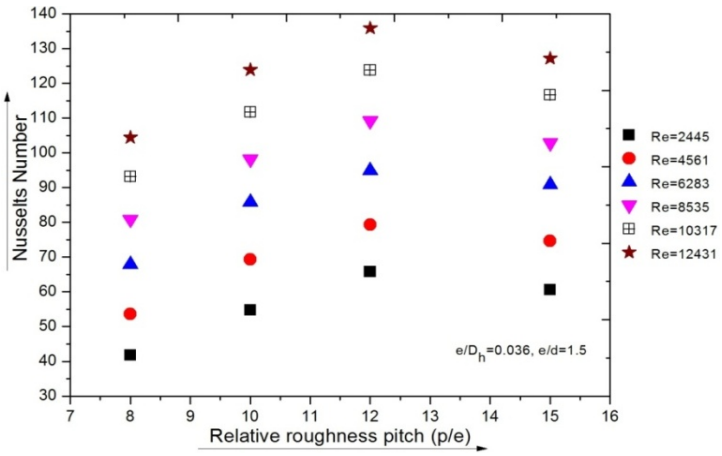

Figure 13: Variation in Nu with p/e for different Re, fixed $e/D_h = 0.036$ and $e/d = 1.5$.

Nu is increased. With increase in p/e value, Nusselt number increases up to $p/e = 12$ beyond which Nu is decreased. Highest and lowest Nu is obtained at p/e 12 and 8 respectively for entire Re investigated. Presence of highest Nu at some particular p/e signifies highest number of reattachment point at this p/e. For p/e less than 12, flow is unlikely to re-attach with surface until it reaches the successive roughness element.

Larger relative roughness pitch ($p/e > 12$) produces lesser reattachment points per unit length that creates strong secondary flow, thereby reducing heat transfer. Table 4 shows percentage variation in Nu with variation in p/e and other parameters fixed for one and three sides roughened ducts. It is clearly evident from Table 4 that highest rise in Nusselt number occurs as p/e increased 10–12.

Table 4: Variation of Nu with p/e.

Constant parameter		Relative roughness pitch p/e range	Nu variation range for roughened duct (%)	
e/D_h	e/d		One side roughened duct	Three sides roughened duct
0.018	1.5	8–10	8.26–15.41	10.41–19.55
		10–12	13.25–22.35	16.52–27.64
		12–15	–(7.26–13.21)	–(11.84–20.47)
0.027	1.5	8–10	11.42–21.76	14.76–29.32
		10–12	15.56–28.34	19.31–34.65
		12–15	–(9.32–17.21)	–(13.48–24.57)
0.036	1.5	8–10	14.59–28.45	19.63–31.56
		10–12	18.44–38.54	23.52–39.86
		12–15	–(12.91–21.82)	–(17.43–29.64)
0.045	1.5	8–10	12.56–25.59	16.86–31.76
		10–12	16.47–32.37	20.60–36.21
		12–15	–(10.81–16.25)	–(14.25–25.35)

5.2 Effect of relative roughness height on Nusselt number

The Nusselt number increases as relative roughness height (e/D_h) increases up to 0.036, beyond that it decreases with further increase in e/D_h value. Nu increases in e/D_h range of 0.018–0.036 and decreases in e/D_h range 0.036–0.045. Development of secondary flow along roughened surface allows main core fluid in addition to secondary flow to move across leading

edge as shown in Fig. 14. Air flowing in contact with roughness element is heated gradually and boundary layer becomes thinner in vicinity of roughness element. Variation in e/D_h gives rise to flow belonging to two regions, partly secondary and partly main flow. Even though main flow is fully developed turbulent flow, there exist thick layer of viscous sub layer that reduces convective heat exchange. Roughness element enables secondary flow to rejoin the main flow, resulting in its acceleration that energizes retarded main flow over the surface. Secondary flow contribution in energizing main flow through roughened duct and introduction of colder fluid in secondary flow in downstream of roughness element results in highest convective heat transfer coefficient at $e/D_h = 0.036$. Table 5 shows percentage variation in Nu of one and three sides roughened ducts with increase in e/D_h and fixed other parameters.

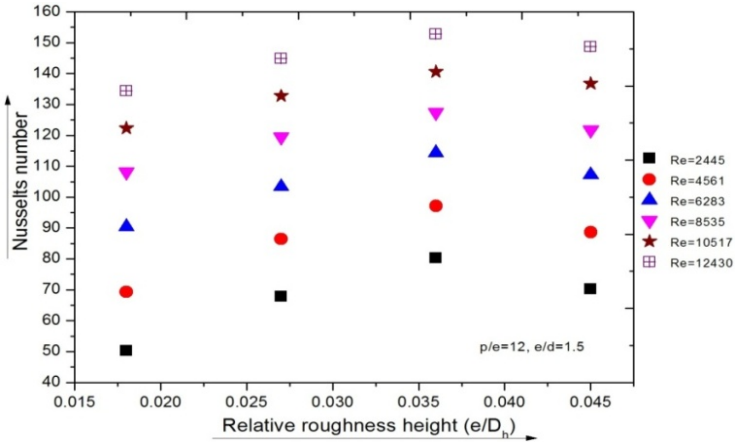

Figure 14: Variation in Nu with e/D_h for different Re and for fixed $p/e = 12$ and $e/d = 1.5$.

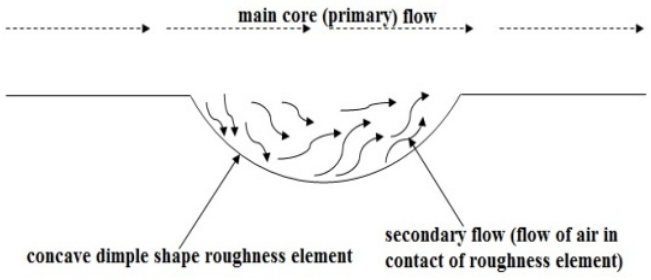

Figure 15: Main and secondary flow pattern [34].

Table 5: Variation in Nu with e/D_h.

Fixed parameter		Relative roughness height e/D_h range	Nu variation range for roughened duct (%)	
p/e	e/d		One side roughened duct	Three sides roughened duct
8	1.5	0.018–0.027	10.13–21.37	13.24–26.43
		0.027–0.036	17.45–31.26	21.46–37.54
		0.036–0.045	–(14.58–24.83)	–(18.78–29.65)
10	1.5	0.018–0.027	12.21–24.10	15.81–29.52
		0.027–0.036	21.62–37.48	25.46–43.63
		0.036–0.045	–(16.46–27.36)	–(21.88–34.28)
12	1.5	0.018–0.027	15.73–29.84	20.16–34.72
		0.027–0.036	26.36–40.81	33.45–48.61
		0.036–0.045	–(20.83–29.54)	–(23.25–32.46)
15	1.5	0.018–0.027	13.87–26.15	16.86–31.76
		0.027–0.036	22.58–36.24	30.47–44.55
		0.036–0.045	–(17.81–27.52)	–(19.15–30.26)

5.3 Effect of relative dimple depth on Nusselt number

Air to be heated significantly; should remain in contact with the roughness as long as highest heat transfer is obtained. To visualize effect of relative dimple depth (e/d) on Nusselt number, Fig. 16 is drawn at constant values of Re and fixed values of other roughness parameters. Larger value of

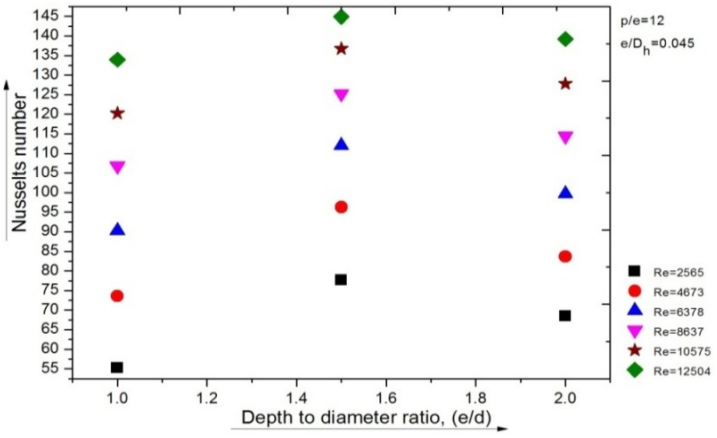

Figure 16: Variation in Nu with e/d for different Re, for fixed $p/e = 12$ and $e/D_h = 0.045$.

depth to diameter ratio ($e/d > 1.5$) would not allow flowing air to escape easily from the roughness element and reattach to main primary flow. For $e/d < 1.5$, air does not remain in contact with the roughness element for sufficiently long time to obtain highest heat transfer. Flow velocities also reduce making it insufficient to accelerate flow through dimples and hence heat transfer may not increase significantly. Less e/d results in insufficient space inside dimples, obstruction to flow may increase that could increase friction across ducts. Thus Nu increases with increase in depth to diameter ratio from 1 to 1.5, and attains maximum at e/d of 1.5. Table 6 and 7 shows

Table 6: Variation in Nusselt number with depth to diameter ratio with varying p/e and fixed e/D_h.

Fixed parameter of roughness geometry		Depth to diameter ratio (e/d) range	Nu variation range for roughened duct (%)	
p/e	e/D_h		One side roughened duct	Three sides roughened duct
8	0.036	1.0–1.5	11.56–19.74	14.23–26.63
		1.5–2.0	–(10.24–16.52)	–(12.32–19.55)
10	0.036	1.0–1.5	13.76–27.59	18.21–31.94
		1.5–2.0	–(12.21–18.82)	–(14.47–22.13)
12	0.036	1.0–1.5	17.44–31.26	21.75–37.84
		1.5–2.0	–(13.29–20.57)	–(16.53–21.45)
15	0.045	1.0–1.5	14.23–19.22	18.78–32.66
		1.5–2.0	–(12.45–17.81)	–(19.27–28.42)

Table 7: Variation of Nusselt number with depth to diameter ratio with varying e/D_h and fixed p/e.

Fixed parameter of roughness geometry		Depth to diameter ratio (e/d) range	Nu variation range for roughened duct (%)	
e/D_h	p/e		One side roughened duct	Three sides roughened duct
0.018	12	1.0–1.5	9.28–16.77	12.57–21.48
		1.5–2.0	–(8.62–13.42)	–(10.44–19.32)
0.027	12	1.0–1.5	14.46–26.17	18.82–32.59
		1.5–2.0	–(11.43–17.33)	–(12.43–20.94)
0.036	12	1.0–1.5	17.44–31.26	21.75–37.84
		1.5–2.0	–(13.29–20.57)	–(16.53–21.45)
0.045	12	1.0–1.5	15.32–27.76	19.54–30.28
		1.5–2.0	–(12.56–18.65)	–(13.83–19.47)

percentage variation in Nu of one and three sides dimple roughened ducts with increase in dimple depth to diameter ratio.

5.4 Enhancement in heat transfer

This section is drafted to visualize effects of roughness provided on three sides to that of one side in terms of the rise in Nusselt number. Nusselt number enhancement ratio is ratio of Nu of three sides to one side roughened duct.

$$\text{Nusselt number enhancement ratio} = \frac{\begin{array}{c}\text{Nusselt no. of three sides concave}\\ \text{dimple roughened duct } (\mathrm{Nu}_{3r})\end{array}}{\begin{array}{c}\text{Nusselt no. of one side concave}\\ \text{dimple roughened duct } (\mathrm{Nu}_{1r})\end{array}}.$$

Augmentation in Nu of 3-sides over 1-side roughened duct is represented by Nu enhancement ratio. Figs. 17 to 19 show variation in Nusselt number enhancement ratio ($\mathrm{Nu}_{3r}/\mathrm{Nu}_{1r}$) as a function of Re and roughness geometry parameters.

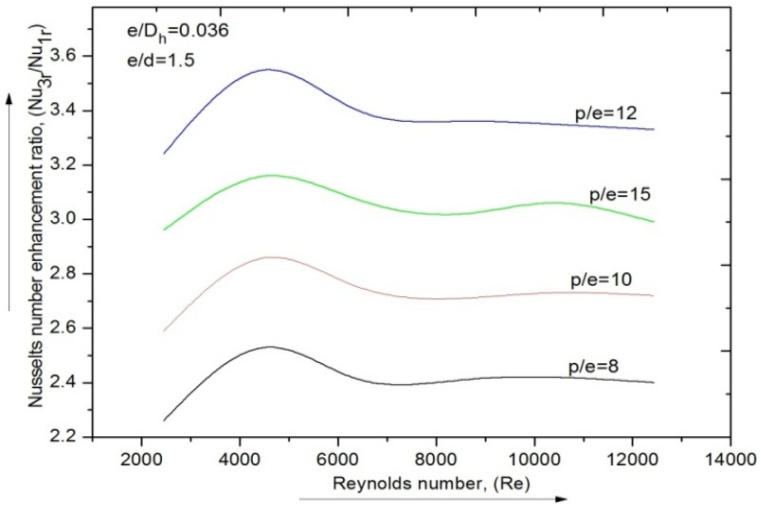

Figure 17: Enhancement ratio ($\mathrm{Nu}_{3r}/\mathrm{Nu}_{1r}$) at varying Re and p/e for fixed $e/D_h = 0.036$ and $e/d = 1.5$.

Highest enhancement in Nu for three sides over one side roughened duct for varying p/e, e/D_h, and e/d is respectively 2.6 to 3.55 times, 1.91 to 3.42 times and 3.09 to 3.94 times. An optimum geometrical parameter value

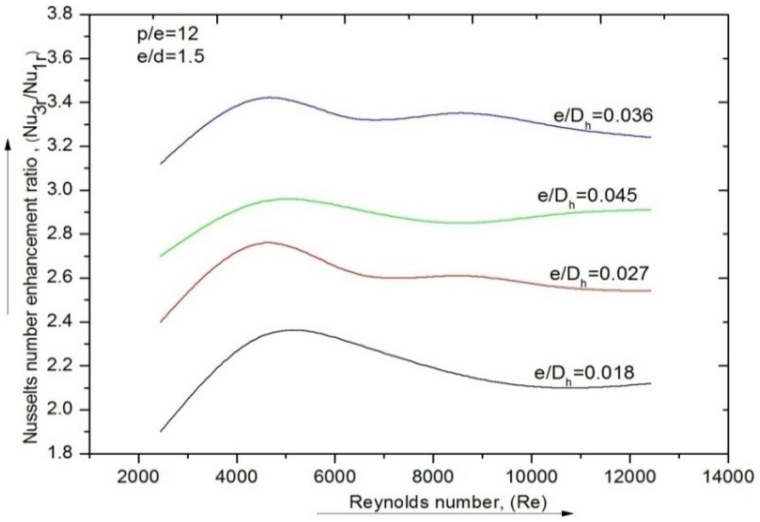

Figure 18: Enhancement ratio ($\mathrm{Nu}_{3r}/\mathrm{Nu}_{1r}$) at varying Re and e/D_h for fixed $p/e = 12$ and $e/d = 1.5$.

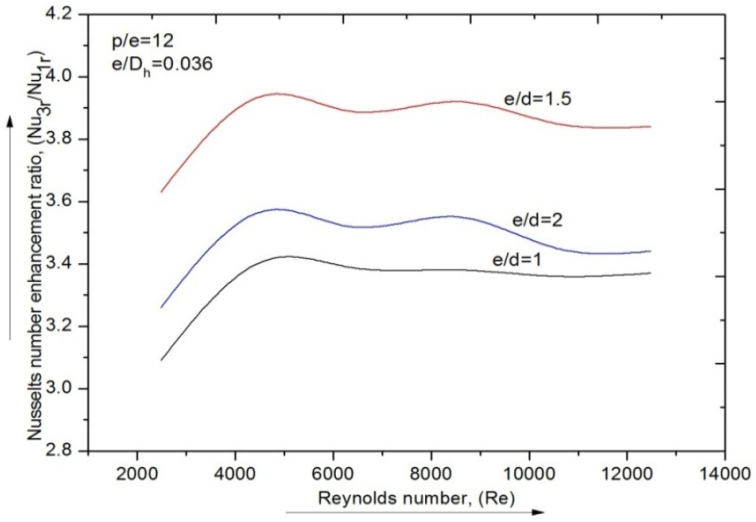

Figure 19: Enhancement ratio ($\mathrm{Nu}_{3r}/\mathrm{Nu}_{1r}$) at varying Re and e/d for fixed $e/D_h = 0.036$ and $p/e = 12$.

(value at which highest Nusselt number is obtained) of p/e, e/D_h, and e/d is obtained. Table 8 shows value of Nusselt number enhancement ratio at optimum flow and roughness parameter.

Table 8: Nusselt number enhancement ratio corresponding to optimum roughness geometry ($p/e = 12$, $e/D_h = 0.036$, $e/d = 1.5$).

Reynolds Number	Nusselt number enhancement ratio
2480	3.63
4590	3.94
6310	3.89
8575	3.92
10558	3.85
12476	3.84

5.5 Effect of relative roughness pitch on friction factor

Rise in heat transfer comes at the cost of increase in friction across roughened ducts. Friction is a very strong function of roughness geometry parameters. To visualize effect of relative roughness pitch (p/e) on friction factor (f), it is plotted against p/e at constant values of Re as shown in Fig. 20. Friction is decreased as Re is increased. Friction decreases monotonously as p/e increases. Highest and lowest friction is observed at p/e of 8 and 15 respectively. This is because as p/e increases, consecutive dimple distance increases that reduces tendency of generation of reattachment points making it difficult for the flow to reattach and move swiftly. Table 9 shows percentage variation in f for one and three sides roughened ducts with varying p/e.

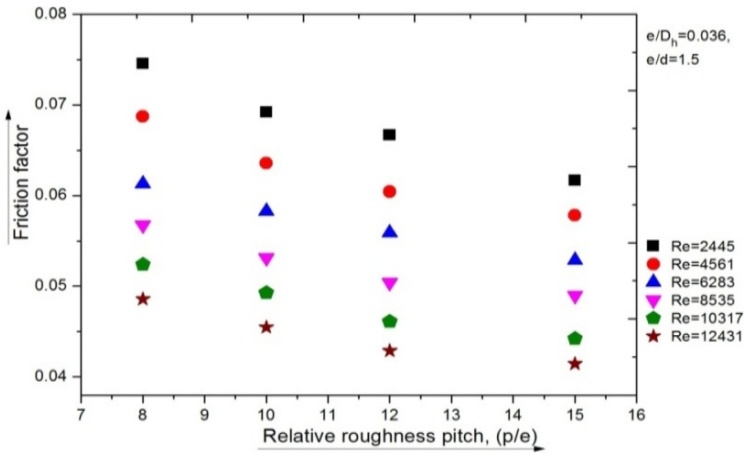

Figure 20: Variation in f with p/e at varying Re, fixed $e/D_h = 0.036$ and $e/d = 1.5$.

Table 9: Variation in f with p/e.

Fixed parameter		Relative roughness pitch p/e range	Friction factor (%)	
e/D_h	e/d		$1r$	$3r$
0.018	1.5	8–10	-(4.24–9.87)	-(6.26–11.25)
		10–12	–(7.55–12.71)	–(9.21–13.42)
		12–15	–(11.42–16.65)	–(14.23–19.37)
0.027	1.5	8–10	–(5.11–11.34)	–(8.62–14.53)
		10–12	–(10.83–17.57)	–(13.27–21.43)
		12–15	–(16.33–21.43)	–(17.43–24.19)
0.036	1.5	8–10	–(4.11–12.42)	–(9.39–16.42)
		10–12	–(9.17–16.84)	–(17.56–24.88)
		12–15	–(15.41–23.59)	–(19.72–28.64)
0.045	1.5	8–10	–(3.47–10.76)	–(8.41–19.26)
		10–12	–(8.29–17.42)	–(17.26–26.32)
		12–15	–(14.22–25.36)	–(22.48–29.87)

5.6 Effect of relative roughness height on friction factor

Variation in friction factor (f) with relative roughness height (e/D_h) for varying Re and constant p/e and e/d is shown in Fig. 21. As e/D_h increases, f monotonously increases for both roughened ducts. Highest and lowest f for roughened ducts is found at $e/D_h = 0.045$ and 0.018, respectively, having $p/e = 8$ and relative dimple depth $e/d = 1.5$. For $e/D_h = 0.036-0.045$, the augmentation in friction is very high; on the contrary Nu decreases.

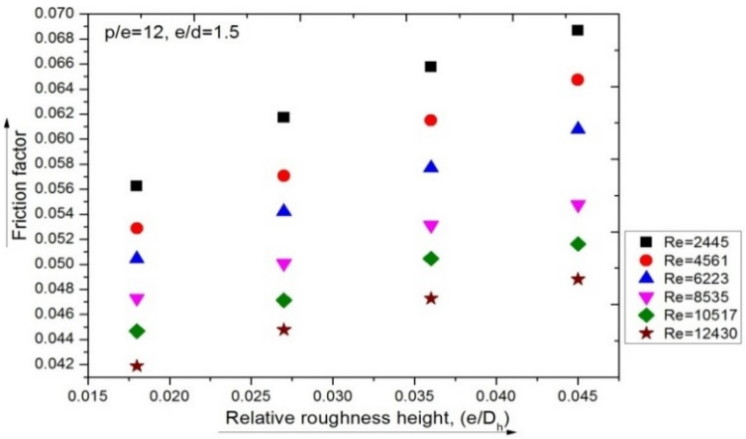

Figure 21: Variation in f with e/D_h for varying Re, fixed $p/e = 12$ and $e/d = 1.5$.

Table 10 shows percentage variation in f for roughened ducts with increase in e/D_h.

Table 10: Variation in f with e/D_h.

Fixed parameter		Relative roughness height e/D_h range	Friction factor (%)	
p/e	e/d		$1r$	$3r$
8	1.5	0.018–0.027	(14.45–19.35)	(19.26–24.88)
		0.027–0.036	(13.55–21.71)	(18.76–27.26)
		0.036–0.045	(15.42–25.65)	(17.23–28.56)
10	1.5	0.018–0.027	(11.11–17.34)	(16.57–25.77)
		0.027–0.036	(10.83–18.57)	(15.22–27.53)
		0.036–0.045	(13.33–22.43)	(16.38–28.19)
12	1.5	0.018–0.027	(10.16–17.62)	(14.54–24.12)
		0.027–0.036	(11.45–19.27)	(15.27–25.46)
		0.036–0.045	(15.38–24.81)	(13.72–27.38)
15	1.5	0.018–0.027	(9.47–16.75)	(10.41–19.26)
		0.027–0.036	(12.43–20.95)	(17.26–28.32)
		0.036–0.045	(11.35–22.15)	(18.48–31.82)

5.7 Effect of dimple depth to diameter ratio on friction factor

Friction factor (f) decreased with increase of up to 1.5 beyond which f increased with increase in depth to diameter. At depth to diameter ratio

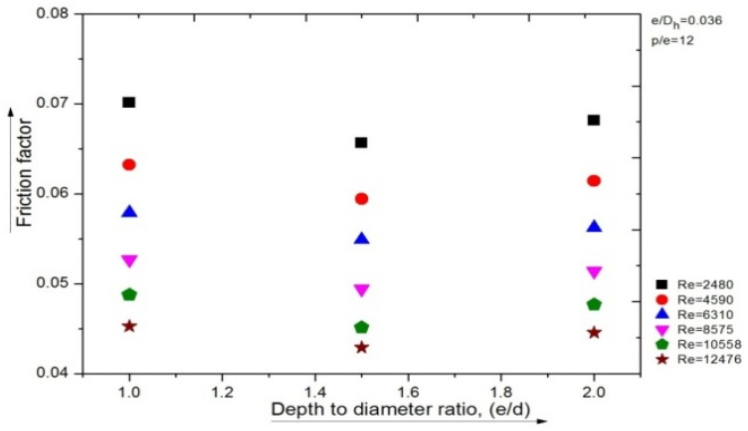

Figure 22: Variation in f with e/d for different Re, fixed $e/D_h = 0.036$ and $p/e = 12$.

$e/d < 1.5$, all dimples take part in flow and pressure drop is considered as cumulative effect of effect produced by individual dimples present on ducts. As depth to diameter ratio $e/d > 1.5$, some dimples do not participate in flow due to less vortices formation. To visualize the effect of e/d, friction factor is plotted against e/d at fixed Reynolds number and other geometrical parameters. Table 11 and 12 shows percentage variation in f with depth to diameter ratio at different sets of roughness geometrical parameter.

Table 11: Variation in f with depth to diameter ratio with varying p/e and fixed e/D_h.

Fixed parameter of roughness geometry		Depth to diameter ratio (e/d) range	Friction factor (f) variation range for roughened duct (%)	
p/e	e/D_h		One side roughened duct	Three sides roughened duct
8	0.036	1.0–1.5	–(7.24–18.52)	–(10.56–24.41)
		1.5–2.0	11.76–17.59	14.25–23.14
10	0.036	1.0–1.5	–(10.51–19.62)	–(13.58–26.56)
		1.5–2.0	12.56–19.71	17.35–26.41
12	0.036	1.0–1.5	–(13.50–21.34)	–(16.62–28.18)
		1.5–2.0	15.42–22.91	19.92–29.85
15	0.036	1.0–1.5	–(15.27–23.74)	–(15.32–25.72)
		1.5–2.0	14.27–19.54	20.65–30.78

Table 12: Variation in f with depth to diameter ratio with varying e/D_h and fixed p/e.

Fixed parameter of roughness geometry		Depth to diameter ratio (e/d) range	Friction factor (f) variation range for roughened duct (%)	
e/D_h	p/e		One side roughened duct	Three sides roughened duct
0.018	12	1.0–1.5	–(10.36–16.61)	–(13.36–20.29)
		1.5–2.0	13.68–21.34	16.38–24.14
0.027	12	1.0–1.5	–(12.75–18.39)	–(14.37–22.78)
		1.5–2.0	16.25–24.69	18.32–28.58
0.036	12	1.0–1.5	–(9.58–18.23)	–(15.61–24.72)
		1.5–2.0	16.45–27.72	19.63–30.45
0.045	12	1.0–1.5	–(11.86–22.94)	–(17.83–27.71)
		1.5–2.0	17.46–30.52	20.24–32.49

5.8 Rise in friction factor

Friction factor rise ratio is ratio of friction of three sides to that of one side dimple roughened duct. It is the measure of quantitative rise in friction of three sides over one side roughened duct.

$$\text{Friction factor rise ratio} = \frac{\text{Friction factor of three sides concave dimple roughened duct } (f_{3r})}{\text{Friction factor of one side concave dimple roughened duct } (f_{1r})}.$$

The rise in friction for roughened ducts of various configurations has been analyzed under similar condition of flow Reynolds number. The rise in friction of three sides over one side roughened ducts with Re for varying parameters like p/e, e/D_h and e/d are respectively depicted in Figs. 23, 24, and 25.

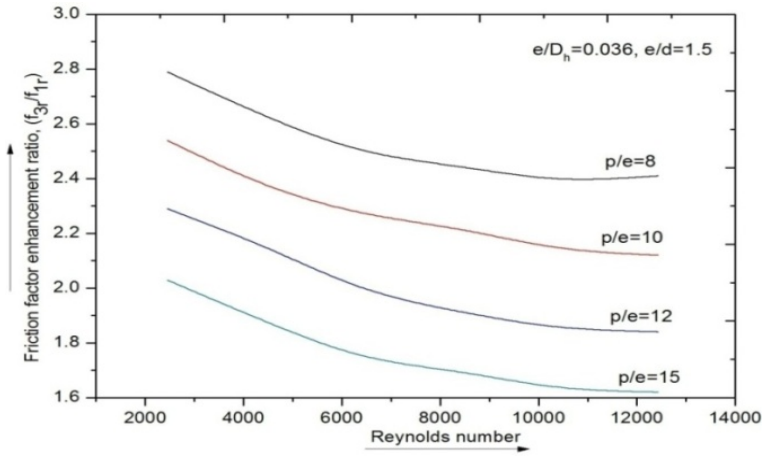

Figure 23: Variation in rise ratio (f_{3r}/f_{1r}) for varying p/e.

Lowest and highest rise in friction of three sides over the one side roughened duct for varying p/e, e/D_h and e/d is respectively 1.62 to 2.79 times, 1.52 to 2.34 times and 2.21 to 2.56 times. Table 13 presents value of friction factor rise ratio at optimum flow and roughness parameter.

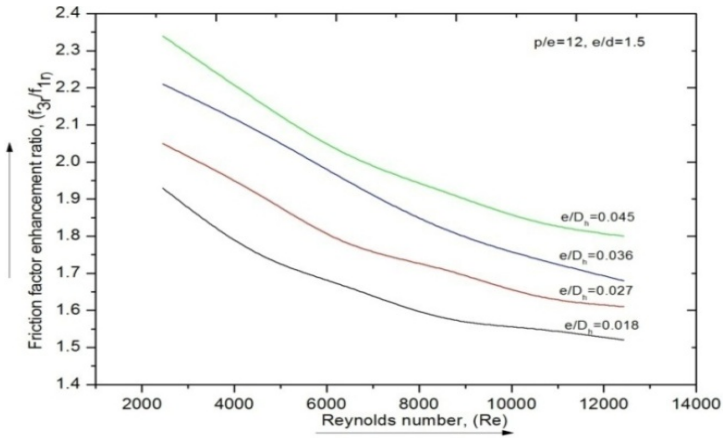

Figure 24: Variation in rise ratio (f_{3r}/f_{1r}) for varying Re for varying e/D_h.

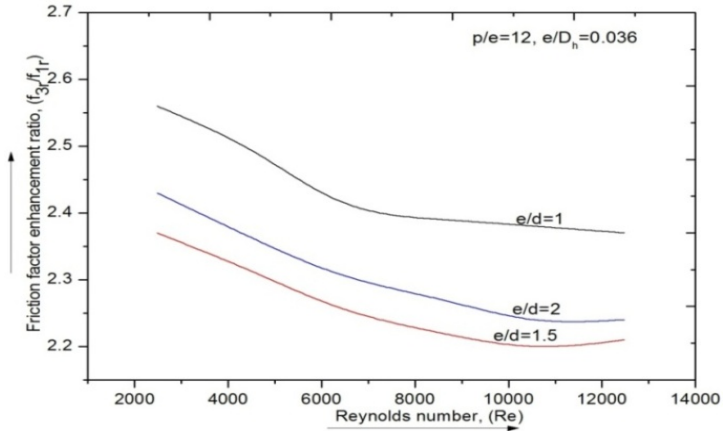

Figure 25: Variation in rise ratio (f_{3r}/f_{1r}) for varying Re for varying e/d.

Table 13: Friction factor rise ratio corresponding to optimum roughness geometry and flow parameter ($p/e = 12$, $e/D_h = 0.036$, $e/d = 1.5$).

Reynolds Number	Friction factor enhancement ratio (f_{3r}/f_{1r})
2480	2.37
4590	2.31
6310	2.26
8575	2.22
10558	2.2
12476	2.21

6 Conclusions

Heat transfer and friction characteristics have been investigated for roughened ducts using concave dimple geometry on one and three sides of absorber plates. Exhaustive experimentation is conducted to record experimental data for Nu and f characteristics. Effects produced by changing roughness and operating parameters on Nu and f characteristics have been determined. The outcomes of present investigations were conclusive and same has been reproduced below:

1. Nu and f varied as p/e, e/D_h and e/d varied under given operating range. In the entire range of Re studied, Nu increased as p/e increased from 8 to 12. On further increasing p/e, Nu decreased for both ducts.

2. Similar trend is found in Nu with variation in e/D_h. Nu increased as e/D_h increased from 0.018 to 0.036, beyond this it decreased for both ducts.

3. Increase in relative dimple depth, e/d from 1 to 1.5 resulted in increase in Nusselt number. Upon increasing e/d from 1.5–2, Nu decreased for both ducts.

4. Highest enhancement in Nu for three sides compared to one side roughened duct for varying p/e, e/D_h and e/d was respectively found as 2.6 to 3.55 times, 1.91 to 3.42 times and 3.09 to 3.94 times.

5. Friction decreased monotonously as p/e varied from 8 to 15 for both ducts.

6. With variation in e/D_h from 0.018–0.045, friction increased monotonously for both ducts.

7. As e/d varied from 1–1.5, friction factor increased. As e/d varied from 1.5 to 2, friction decreased for both ducts.

8. Highest rise in friction of 3-sides over 1-side roughened duct for varying p/e, e/D_h and e/d was respectively 1.62 to 2.79 times, 1.52 to 2.34 times and 2.21 to 2.56 times.

Received 9 February 2019

References

[1] Sukhatme S.P.: *Solar Energy Engineering*. Prentice Hall Inc., New Jersey 1986.

[2] Han J.C., Zhang, Y.M., Lee C.P.: *Augmented heat transfer in square channels with parallel, crossed, and V shaped angled ribs*. J. Heat Trans-T ASME **113**(1991), 590–596.

[3] Han J.C., Park J.S., Lei C.K.: *Heat transfer in rectangular channel with rib-turbulators*. Int. J. Heat Mass Tran. **31**(1984), 183–195.

[4] Saini J.S.: *Use of artificial roughness for enhancing performance of solar air heater*. Proc. XVII National and VI ISHME/ASME Heat and Mass Transfer Conference, January 05–07, 2004. IGCAR, Kalpakkam, India.

[5] Duffie J.A., Beckman W.A.: *Solar Engineering Thermal Processes*. John Wiley, New York 1991.

[6] Garg H.P., Prakash J.P.: Solar Energy – Fundamentals and Applications, Tata McGraw-Hill, New Delhi, 1997.

[7] Panos K., Ehab S., Farrinton D.: *Effect of artificial roughness on heat transfer and friction factor in a solar air heater*. Sol. Energy **3**(1959), 19–23.

[8] Han J.C., Glicksman L.R., Rosenow W.M.: *Investigation of heat transfer and friction for rib-roughened surfaces*. Int. J. Heat Mass Tran. **21**(1978), 1143–56.

[9] Lau S.C., McMillin R.D., Han J.C.: *Turbulent heat transfer and friction in a square channel with discrete rib turbulators*. Trans ASME, J Turbo Machinery **113**(1991), 360–366.

[10] Alam T., Kim M.: *Numerical study on thermal hydraulic performance improvement in solar air heater duct with semi ellipse shaped obstacles*. Energy **112**(2016), 588–598.

[11] Dhiman P., Thakur N.S., Chauhan S.R.: *Thermal and thermohydraulic performance of counter and parallel flow packed bed solar air heaters*. Renew. Energy **46**(2012), 259–268.

[12] Ravi R.K., Saini R.P.: *Experimental investigation on performance of a double pass artificial roughened solar air heater duct having roughness elements of the combination of discrete multi V shaped and staggered ribs*. Energy **116**(2016), 507–516.

[13] Prasad B.N., Saini J.S.: *Effect of artificial roughness on heat transfer and friction factor in a solar air heater*. Sol. Energy **41**(1988), 6, 555–560.

[14] Ravigururajan T.S., Bergles A.E.: *General correlations for pressure drop and heat transfer for single-phase turbulent flow in internally ribbed tubes*. Trans. ASME HTD **52(**1985), 9–20.

[15] Saini R. P. and Saini J.S.: *Heat transfer and friction factor correlations for artificially roughened ducts with expanded metal mesh as roughness element*. Int. J. Heat Mass Tran. **40**(1997), 4, 973–986.

[16] Momin A.M.E., Saini J.S., Solanki S.C.: *Heat transfer and friction in solar air heater duct with V-shaped rib roughness on absorber plate*. Int. J. Heat Mass Tran. **45**(2002), 3383–3396.

[17] Karmare S.V., Tikekar A.N.: *Heat transfer and friction factor correlation for artificially roughened duct with metal grit ribs*. Int. J. Heat Mass Tran. **50**(2007), 4342–4351.

[18] Chandra P.R., Alexander C.R., Han J.C.: *Heat transfer and friction behaviors in rectangular channel with varying number of ribbed walls*. Int. J. Heat Mass Tran. **46**(2003), 481–495.

[19] Burgess N.K., Oliveira M.M., Ligrani P.M.: *Nusselts number behavior on deep dimpled surfaces with a channel*. J. Heat Transfer **125**(2003), 11–18.

[20] Ridouane E.I.H., Campo A.: *Heat transfer and pressure drop characteristics of laminar air flows moving in a parallel-plate channel with transverse hemi-cylindrical cavities*. Int. J. Heat Mass Tran. **50**(2007), 3913–3924.

[21] Karwa R., Solanki S.C., Saini J.S.: *Heat transfer coefficient and friction factor correlation for the transitional flow regime in rib-roughened rectangular duct*. Int. J. Heat Mass Tran. **42**(1999), 1597–1615.

[22] Jaurker A.R., Saini J.S., Gandhi B.K.: *Heat transfer and friction characteristics of rectangular solar air heater duct using rib-grooved artificial roughness*. Sol. Energy **80**(2006), 895–907.

[23] Saini S.K., Saini R.P.: *Development of correlations for Nusselts number and friction factor for solar air heater with roughened duct having arc-shaped wire as artificial roughness*. Sol. Energy **82**(2008), 1118–1130.

[24] Wongcharee K., Changcharoen W., Eiamsa-ard S.: *Numerical investigation of flow friction and heat transfer in a channel with various shaped ribs mounted on two opposite ribbed walls*. Int. J. Chem. React. Eng. **9**(2011), 1–21.

[25] Varun, Saini R.P., Singal S.K.: *Investigation on thermal performance of solar air heaters having roughness elements as a combination of inclined and transverse ribs on the absorber plate*. Renew. Energy **33**(2008), 1398–1405.

[26] Kumar V., Prasad L.: *Thermal performance investigation of one and three sides concave dimple roughened solar air heaters*. IJMET **8**(2017), 12, 31–45, ID: IJMET_08_12_004.

[27] Kumar V., Prasad L.: *Experimental investigation on heat transfer and fluid flow of air flowing under three sides concave dimple roughened duct*. IJMET **8**(2017), 11, 1083–1094, ID: IJMET_08_11_110.

[28] Kumar V., Prasad L.: *Experimental analysis of heat transfer and friction for three sides roughened solar air heater*. Annales de Chimie – Science des Matériaux, 75–107, ACSM. Volume 41–n°C 1–2/2017.

[29] Kumar V.: *Nusselt number and friction factor correlations of three sides concave dimple roughened solar air heater*. Renew. Energy **135**(2019), 355–377.

[30] Kumar V., Prasad L.: *Performance Analysis of three sides concave dimple shape roughened solar air heater*. J. Sustainable Development of Energy, Water and Environment Systems JSDEWES **6**(2018), 4, 631–648.

[31] Kumar V., Prasad L.: *Performance prediction of three sides hemispherical dimple roughened solar duct*. Instrumentation, Mesure, Métrologie I2M. **17**(2018), 2, 273–293.

[32] Kumar V., Prasad L.: *Augmentation in thermal efficiency of three sides over one side concave dimple roughened ducts*. Carbon – Sci. Tech. **10**(2018), 3, 8–16, ISSN 0974-0546.

[33] Kumar V., Prasad L.: *Thermal performance investigation of three sides concave dimple roughened solar air heaters*. Sol. Energy **188**(2019), 361–379.

[34] ASHRAE Standard 93–97, *Methods of testing to determine the thermal performance of solar collectors*. American Society of Heating, Refrigerating and Air-conditioning Engineers Inc., Atlanta, 1977.

[35] Saini R.P., Verma J.: *Heat transfer and friction correlations for a duct having dimple shape artificial roughness for solar air heater*. Energy **33**(2008), 1277–1287.

[36] Kline S.J., McClintock F.A.: *Describing uncertainties in single sample experiments*. Mech. Eng. **75**(1953), 3–8.

[37] Murmu R., Kumar P., Singh H.N.: *Heat transfer and friction factor correlation for inclined spherical ball roughened solar air heater*. Arch. Thermodyn. **41**(2020), 2, 3–34, doi: 10.24425/ather.2020.132958

APPENDIX-A

Uncertainty Analysis and measurement uncertainty

The experimental data recorded during investigation often differ from the actual data due to a lot of unaccountable factors while performing experiments. This deviation of the recorded data from actual data is called as uncertainty. The uncertainty is determined using method suggested by Klein and McClintock [36]. The procedure for the evaluation of uncertainty has been discussed below:

Let a parameter be calculated using certain measured quantities as,

$$y = -y(x_1, x_2, x_3, \ldots, x_n).$$

Then uncertainty in measurement of y is given as follows:

$$\delta_y = \left[\left(\frac{\delta_y}{\delta_{x_1}} \delta_{x_1} \right)^2 + \left(\frac{\delta_y}{\delta_{x_2}} \delta_{x_2} \right)^2 + \left(\frac{\delta_y}{\delta_{x_3}} \delta_{x_3} \right)^2 + \ldots + \left(\frac{\delta_y}{\delta_{x_n}} \delta_{x_n} \right)^2 \right]^{0.5}, \quad \text{(A1)}$$

where δ_{x_1}, δ_{x_2}, δ_{x_3}, …, δ_{x_n} are the possible errors in measurements of $x_1, x_2, x_3 \ldots x_n$.

The value δ_y is absolute uncertainty and $\dfrac{\delta_y}{y}$ is relative uncertainty.

Uncertainty in the measurement of various parameters:

1. Area of flow, plate and orifice meter

Area of absorber plate ($A_p = W \times L$):

$$\frac{\delta A_p}{A_p} = \left[\left(\frac{\delta L}{L}\right)^2 + \left(\frac{\delta W}{W}\right)^2\right]^{0.5}; \tag{A2}$$

$$\frac{\delta A_p}{A_p} = \left[\left(\frac{1.1}{1500}\right)^2 + \left(\frac{0.06}{250}\right)^2\right]^{0.5} = 0.0007716\,.$$

Cross sectional area of air flow duct (A):

$$\frac{\delta A}{A} = \left[\left(\frac{\delta H}{H}\right)^2 + \left(\frac{\delta W}{W}\right)^2\right]^{0.5}; \tag{A3}$$

$$\frac{\delta A}{A} = \left[\left(\frac{0.04}{25}\right)^2 + \left(\frac{0.06}{250}\right)^2\right]^{0.5} = 0.001617.$$

Area of orifice meter (A_o):

$$\begin{aligned} \frac{\delta A_o}{A_o} &= \left[\frac{\left(\dfrac{\pi D_o \times \delta D_o}{2}\right)}{\dfrac{\pi D_o^2}{4}}\right]^{0.5}, \\ \frac{\delta A_o}{A_o} &= \left[\frac{2\delta D_o}{D_o}\right]; \\ \frac{\delta A_o}{A_o} &= \left[\frac{2 \times 0.04}{38}\right] = 0.002105. \end{aligned} \tag{A4}$$

2. Hydraulic diameter

$$\frac{\delta D_h}{D_h} = \frac{\left[\left(\dfrac{\delta D_h \delta W}{W}\right)^2 + \left(\dfrac{\delta D_h \delta H}{H}\right)^2\right]^{0.5}}{[2(W \times H)(W + H)]^{-1}}; \tag{A5}$$

$$\frac{\delta D_h}{D_h} = \frac{\left[\left(\dfrac{0.04 \times 0.06}{250}\right)^2 + \left(\dfrac{0.04 \times 0.04}{25}\right)^2\right]^{0.5}}{[2\,(250 \times 25)\,(250 + 25)]^{-1}} = 0.002321.$$

3. Density

$$\frac{\delta\rho_a}{\rho_a} = \left[\left(\frac{\delta P_a}{P_a}\right)^2 + \left(\frac{\delta T_o}{T_o}\right)^2\right]^{0.5}; \tag{A6}$$

$$\frac{\delta\rho_a}{\rho_a} = \left[\left(\frac{0.2}{101}\right)^2 + \left(\frac{0.41}{39}\right)^2\right]^{0.5} = 0.00106.$$

4. Mass flow rate

$$\frac{\delta\dot{m}}{\dot{m}} = \left[\left(\frac{\delta C_d}{C_d}\right)^2 + \left(\frac{\delta A_o}{A_o}\right)^2 + \left(\frac{\delta\rho_a}{\rho_a}\right)^2 + \left(\frac{\delta\Delta P_o}{P_o}\right)^2\right]^{0.5}; \tag{A7}$$

$$\frac{\delta\dot{m}}{\dot{m}} = \left[\left(\frac{0.005}{0.62}\right)^2 + (0.002105)^2 + (0.00106)^2 + \left(\frac{0.14}{354}\right)^2\right]^{0.5} = 0.008411.$$

5. Velocity of air through test section

$$V = \frac{\dot{m}}{\rho(WH)}, \tag{A8}$$

$$\frac{\delta V}{V} = \left[\left(\frac{\delta\dot{m}}{\dot{m}}\right)^2 + \left(\frac{\delta\rho}{\rho}\right)^2 + \left(\frac{\delta W}{W}\right)^2 + \left(\frac{\delta H}{H}\right)^2\right]^{0.5};$$

$$\frac{\delta V}{V} = \left[(0.008411)^2 + (0.00106)^2 + \left(\frac{0.06}{250}\right)^2 + \left(\frac{0.04}{25}\right)^2\right]^{0.5} = 0.00863.$$

6. Reynolds Number (Re)

$$\mathrm{Re} = \frac{\rho V D_h}{\mu}, \tag{A9}$$

$$\frac{\delta\mathrm{Re}}{\mathrm{Re}} = \left[\left(\frac{\delta V}{V}\right)^2 + \left(\frac{\delta\rho}{\rho}\right)^2 + \left(\frac{\delta D_h}{D_h}\right)^2 + \left(\frac{\delta\mu}{\mu}\right)^2\right]^{0.5};$$

$$\frac{\delta\mathrm{Re}}{\mathrm{Re}} = \left[(0.00863)^2 + (0.00106)^2 + (0.002321)^2 + \left(\frac{0.002}{1.89}\right)^2\right]^{0.5} = 0.009061.$$

7. Useful heat gain

$$\frac{\delta Q_u}{Q_u} = \left[\left(\frac{\delta \dot{m}}{\dot{m}}\right)^2 + \left(\frac{\delta C_p}{C_p}\right)^2 + \left(\frac{\delta \Delta T}{\Delta T}\right)^2\right]^{0.5}; \tag{A10}$$

$$\frac{\delta Q_u}{Q_u} = \left[(0.008411)^2 + \left(\frac{1.4}{1005}\right)^2 + \left(\frac{0.68}{22.48}\right)^2\right]^{0.5} = 0.03142\,.$$

8. Heat transfer co-efficient

$$\frac{\delta h}{h} = \left[\left\{\frac{\delta Q}{Q}\right\}^2 + \left\{\frac{\delta A_p}{A_p}\right\}^2 + \left\{\frac{\delta (T_{pm})}{(T_{pm})}\right\}^2\right]^{0.5}; \tag{A11}$$

$$\frac{\delta h}{h} = \left[\{0.03144\}^2 + \{0.0007716\}^2 + \left\{\frac{0.19}{(28.13)}\right\}^2\right]^{0.5} = 0.03724.$$

9. Nusselt number

$$\frac{\delta \mathrm{Nu}}{\mathrm{Nu}} = \left[\left\{\frac{\delta h}{h}\right\}^2 + \left\{\frac{\delta D_h}{D_h}\right\}^2 + \left\{\frac{\delta (k)}{(k)}\right\}^2\right]^{0.5}; \tag{A12}$$

$$\frac{\delta \mathrm{Nu}}{\mathrm{Nu}} = \left[\{0.03724\}^2 + \{0.002321\}^2 + \left\{\frac{\delta (0.00001)}{(0.02652)}\right\}^2\right]^{0.5} = 0.04167.$$

10. Friction factor

$$\frac{\delta f}{f} = \left[\left\{\frac{\delta (\Delta p_d)}{(\Delta p_d)}\right\}^2 + \left\{\frac{\delta D_h}{D_h}\right\}^2 + \left\{\frac{\delta (L)}{L}\right\}^2 + \left\{\frac{\delta (V)}{V}\right\}^2 + \left\{\frac{\delta (\rho)}{\rho}\right\}^2\right]^{0.5}; \tag{A13}$$

$$\frac{\delta f}{f} = \left[\left\{\frac{(0.01)}{(10)}\right\}^2 + \{0.002321\}^2 + \left\{\frac{(0.87)}{1500}\right\}^2 + \{0.00863\}^2 + \{0.00106\}^2\right]^{0.5} = 0.04389.$$

The uncertainty analysis has been carried out for the entire set of parameter investigated within the operating range and the uncertainty variation of various parameters obtained is presented in Tabs. 2 and 3.